CASL-U-2013-0193-000

Power uprates
and plant life extension

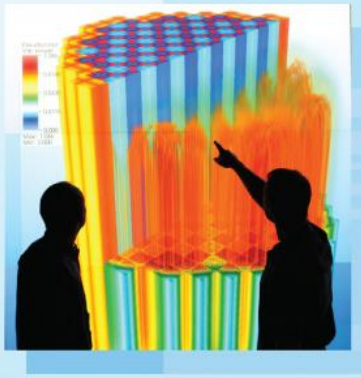

Engineering design
and analysis

Science-enabling
high performance
computing

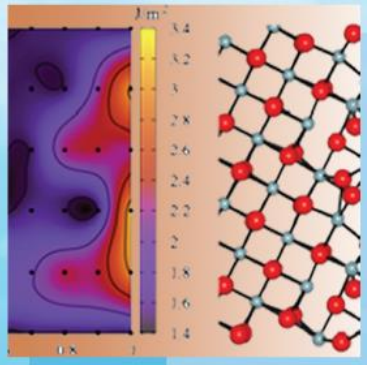

Fundamental science

Plant operational data

Consortium for Advanced Simulation of LWRs

L3:THM.CFD.P7.06 Implementation and validation of the new RPI boiling models using STAR-CCM+ as CFD Platform

Victor Petrov, Annalisa Manera
UMICH

September 30, 2013

U.S. DEPARTMENT OF ENERGY | Nuclear Energy

EXECUTIVE SUMMARY

This milestone is focused on the assessment of the new boiling models developed by the RPI team. The RPI models have been originally developed and tested using NPHASE as the base Computational Fluid Dynamics (CFD) solver.

In order to gain experience for the further implementation of these models in the VERA CFD tool HYDRA-TH, the RPI models have been implemented in the commercial CFD software STAR-CCM+.

In the present milestone we report about the implementation of the new RPI models in STAR-CCM+, the assessment of the behavior of the new RPI models when executed from a CFD platform other than NPHASE, and the validation of the models against selected experimental data.

CONTENTS

1 MILESTONE DESCRIPTION 9
1.1 RPI closure modeling background 9

2 SELECTED EXPERIMENTAL TESTS 10
2.1 Bartolomei's test 10
2.2 DEBORA's tests 10

3 BOILING MODELS FOR SUBCOOLED FLOWS 11
3.1 New RPI model 11
3.1.1 Bubble hydrodynamics 11
3.1.2 Interfacial heat transfer 12
3.1.3 WALL HEAT TRANSFER (HEAT PARTITIONING FOR FORCED CONVECTION SUBCOOLED BOILING) 13
3.2 STAR-CCM+ reference boiling models 14

4 ASSESSMENT OF BOILING MODELS AGAINST EXPERIMENTS 16
4.1 Comparison of STAR-CCM+ reference model with RPI-NPHASE 16
4.2 Implementation of the new RPI model in STAR-CCM+ and assessment against Bartolomei's experiment 17
4.3 Implementation of the new RPI model in STAR-CCM+ and assessment against selected DEBORA's experiments 20

5 CONCLUSIONS AND FUTURE WORK 27

6 REFERENCES 27

FIGURES

Figure 1 Scheme of the Bartolomei experimental set-up (where: 1 – Surface heater, 2 – contact heater, 3 – transformer, 4 – experimental section, 5 – separator). 10

Figure 2 Scheme of the DEBORA experimental set-up 11

Figure 3: Performance of the new RPI model implemented in NPHASE and the reference STAR-CCM+ model against the Bartolomei experiment. Left: cross-section averaged liquid temperature as function of elevation; right: wall temperature (Tw) and liquid centerline temperature (Tcl) as function of elevation. 16

Figure 4: Performance of the new RPI model implemented in NPHASE and the reference STAR-CCM+ model against the Bartolomei experiment. Left: cross-section averaged void fraction as function of elevation; right: void fraction radial distribution at the test section outlet. 16

Figure 5: Performance of the new RPI model implemented in STAR-CCM+ and STAR-CCM+ model against the Bartolomei experiment - effect of gas-liquid interface to liquid heat transfer on liquid and wall temperatures. 18

Figure 6: Performance of the new RPI model implemented in STAR-CCM+ and STAR-CCM+ model against the Bartolomei experiment - effect of gas-liquid interface to liquid heat transfer on the void fraction. 18

Figure 7: Performance of the new RPI model implemented in STAR-CCM+ and STAR-CCM+ model against the Bartolomei experiment - effect of bubble departure diameter on liquid and wall temperatures. 19

Figure 8: Performance of the new RPI model implemented in STAR-CCM+ and STAR-CCM+ model against the Bartolomei experiment - effect of bubble departure diameter on the void fraction. 19

Figure 9: Performance of the new RPI model implemented in STAR-CCM+ and STAR-CCM+ model against the Bartolomei experiment - effect of heat partitioning on liquid and wall temperatures. 20

Figure 10: Performance of the new RPI model implemented in STAR-CCM+ and STAR-CCM+ model against the Bartolomei experiment - effect of heat partitioning on the void fraction. 20

Figure 11: Computational results for DEB13 (left) and C4 (right) cases. 22

Figure 12: Computational results for S4 (left) and C6 (right) cases. 23

Figure 13: Color bar for Figure 14 to Figure 16. 24

Figure 14: Void-fraction profiles for different variants of boiling models – DEB13.....25

Figure 15: Void-fraction profiles for different variants of boiling models - C4.....25

Figure 16: Void-fraction profiles for different variants of boiling models - S4 26

Figure 17: Void-fraction profiles for different variants of boiling models – C6 26

Figure 18: Wall temperature profile for case S4 model variant #02 (STAR-CCM+ reference model with Bozzano-Dante's correlation for the drag coefficient). 27

TABLES

Table 1 - Selected test cases of the DEBORA experimental campaign.....11

NOMENCLATURE

D_b = bubble diameter
k = turbulent kinetic energy
k_l = liquid thermal conductivity
ρ = density
u_r = relative gas velocity

<u>Subscripts</u>
l = liquid
g = gas

1 MILESTONE DESCRIPTION

This milestone is focused on the assessment of the new boiling models developed by the RPI team. The RPI models have been originally developed and tested using NPHASE as the base Computational Fluid Dynamics (CFD) solver.

In order to gain experience for the further implementation of these models in the VERA CFD tool HYDRA-TH, the RPI models have been implemented in the commercial CFD software STAR-CCM+.

In the present milestone we report about the implementation of the new RPI models in STAR-CCM+, the assessment of the behavior of the new RPI models when executed from a CFD platform other than NPHASE, and the validation of the models against selected experimental data.

1.1 RPI closure modeling background

The contribution of the RPI group to THM has been specifically directed towards the continuous improvement of closure modeling for subcooled flow boiling. A specific milestone (L3:THM.CLS.P6.02) was completed to support the current work. The RPI activities, which have been used as basis for the present work were focused on:

- development of a new improved local model for predicting the heated wall temperature in subcooled boiling.
- formulation of closure laws for the near wall combined evaporation and condensation phenomena.
- model validation against selected experimental data.

The work at RPI has provided a considerable advancement in the understanding of the wall boiling modeling behavior. The scope of this milestone has therefore been to implement these findings in the commercial tool STAR-CCM+ and assess their efficiency in order to establish a robust baseline.

2 SELECTED EXPERIMENTAL TESTS

2.1 Bartolomei's test

The Bartolomei experimental set-up [1] comprises an open loop connected to an inlet water supply and an outlet superheated steam line. The test section consists of a circular pipe with an inner diameter of 15.4 mm and a heated length of 2m. The test section wall is heated by means of electrical current. Subcooled water is pre-heated by means of steam to the required temperature before entering the heated channel. The experimental test used in the present report was carried at 45 bar, with an inlet mass flux of 900 kg/m^{2}s, an inlet subcooling of 60 K and a wall heat flux of 0.57 MW/m^2.

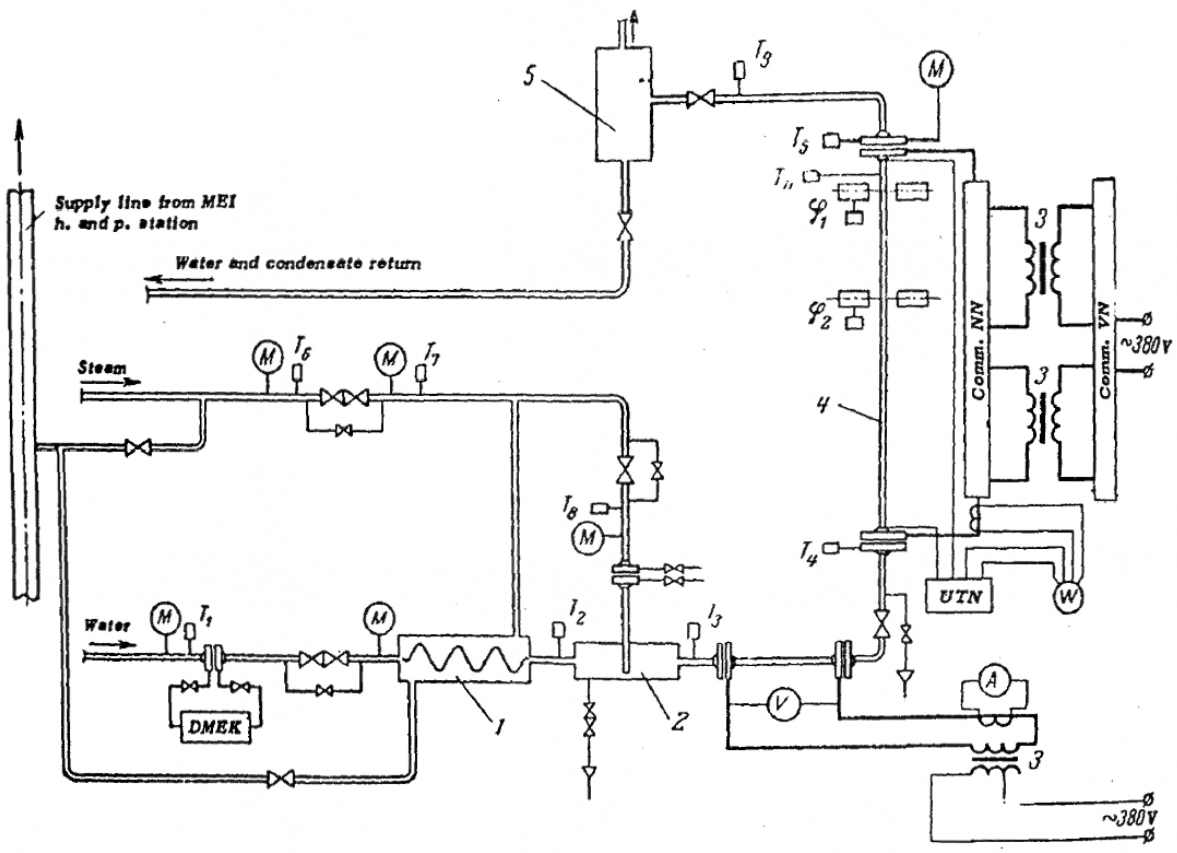

Figure 1 Scheme of the Bartolomei experimental set-up (where: 1 – Surface heater, 2 – contact heater, 3 – transformer, 4 – experimental section, 5 – separator).

2.2 DEBORA's tests

In the DEBORA experimental campaign [2] Dichlorodifluoromethane (R12) was used as the working medium. The test section consists of a heated circular pipe having a inner diameter of 19 mm, and a heated length of 3.5 m followed by a 0.5 m adiabatic section. A scheme of the experimental set-up is shown in Figure 2. The operational conditions of the DEBORA test cases used in the present report for the validation of the new RPI models implemented in STAR-CCM+ are listed in Table 1.

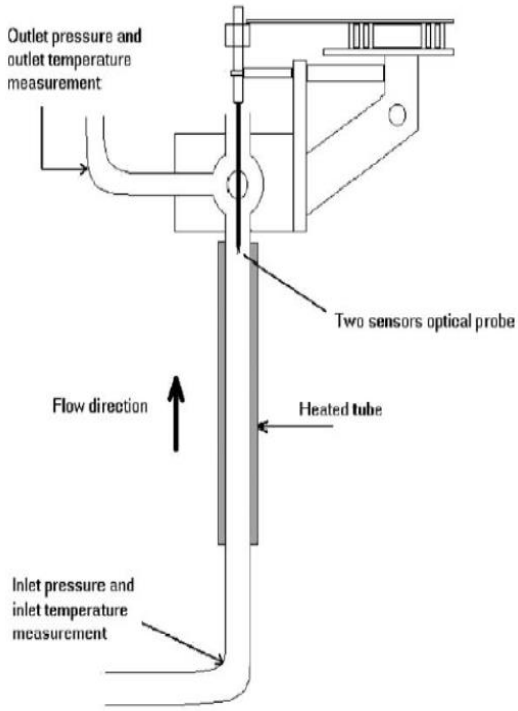

Figure 2 Scheme of the DEBORA experimental set-up

Table 1 - Selected test cases of the DEBORA experimental campaign

Case	Pressure, (bar)	Heat flux, (m/s)	V(inlet), (m/s)	T(inlet), (K)	Tsat, (K)
DEB13	26.17	109420	2.63	342.35	359.921
S4	26.15	72722	1.76	343.68	359.881
DEB_C 4	30.08	58260	0.88	341.04	367.392
DEB_C 6	30.07	58260	0.90	345.8	367.374

3 BOILING MODELS FOR SUBCOOLED FLOWS

3.1 New RPI model

While the basic equations of the Eulerian M-CFD are not include here for sake of brevity as they are later discussed in the CFD tool development section, the assembled reference closure is reported in sections 3.1.1 to 3.1.3. The equations were gathered from Refs. [3-6]

3.1.1 Bubble hydrodynamics

<u>Drag force</u>

The drag force acting on the bubbles is given by:

(1) $$\overrightarrow{F_D} = -\frac{3}{4}\frac{C_D}{D_b}\alpha\rho_l|\vec{u}_v - \vec{u}_l|(\vec{u}_v - \vec{u}_l)$$

where the drag coefficient used in most two-phase flow formulations is the one computed for a sphere:

(2) $$C_D = \frac{24}{Re_b}\left(1 + 0.1 Re_b^{0.75}\right)$$

With the bubble Reynolds number defined as:

(3) $$Re_b = \frac{\rho_l |\vec{u}_v - \vec{u}_l| D_b}{\mu_b}$$

with D_b being the bubble diameter. The drag coefficient is modified in the RPI model according to the following correlation:

(4) $$C_D = \frac{24}{Re_b}\left(1 + 0.092 Re_b^{0.78}\right)$$

Lift force

The force acting on the bubbles is given by:

(5) $$\vec{F_L} = -C_L \alpha \rho_l |\vec{u}_v - \vec{u}_l| \times \left(\vec{\nabla} \times \vec{u}_l\right)$$

where the lift coefficient C_L is case dependent. For the Bartolomei case included in the model assessment reported in the next chapters, a coefficient $C_L = 0.03$ was used.

In the RPI model, the lift force is applied at a distance from the wall greater than one bubble diameter. For smaller distances, the calculations of void fraction based on force balance are invalid, so it is assumed that the lift coefficient is zero in that region. Alternative models reported in the literature do not assume the lift force to be zero close to the wall, but they do compensate with the so-called Antal's force, which pushes the bubbles away from the wall.

Turbulent dispersion force

(6) $$\vec{F}_{TD} = -C_{TD} \alpha \rho_l \bar{\bar{k}}_l \nabla \alpha$$

where $\underline{\underline{\kappa}}_l = \overline{(u'_{l,i} u'_{l,j})}\delta_{ij}$ for i,j=1,2,3, and δ_{ij} is the Kronecker delta.

with $C_{TD} = \frac{2}{3}$

Virtual mass

(7) $$\vec{F}_{vm} = -C_{vm} \alpha \rho_l \left(\frac{D\vec{u}_v}{Dt} - \frac{D\vec{u}_l}{Dt}\right)$$

with $C_{vm} = 0.5$

3.1.2 Interfacial heat transfer

In the current version of the model, bubbles are assumed to be spherical. Therefore, the interfacial area density is given by:

(8) $a_i = \frac{6\alpha}{D_b}$

It is assumed that the temperature of the vapour-liquid interface is equal to saturation (Tsat). The heat transfer rate between interface and phase j is equal to:

(9) $q_j''' = N''' A_s h_j (T_{sat} - T_j)$

with:

N''' = bubble number density defined as $N''' = \frac{\alpha}{V_b}$

A_s = bubble surface area defined equal to πD_b^2

h_j = heat transfer coefficient between interface and phase j

For the liquid phase, the heat transfer coefficient hl is defined according to the following Nusselt number correlation:

(10) $Nu = C_{vol}\left[2 + \left(0.4Re_b^{0.5} + 0.06Re_b^{2/3}\right)\right]Pr_l^{0.4} = \frac{h_l D_b}{k_l}$

where C_{vol} is a correction factor to take into account condensation (=1 for single sphere, > 1 because of bubble-induced turbulence). This correction will require further evaluation.

It is further assumed that the heat transfer coefficient between the gas-liquid interface and the gas phase is null.

3.1.3 WALL HEAT TRANSFER (HEAT PARTITIONING FOR FORCED CONVECTION SUBCOOLED BOILING)

The heat partitioning is decomposed into two components, a boiling component (which includes evaporation and quenching) and a single-phase component respectively:

(11) $q_w'' = q_b'' + q_{1\phi}''$

The single-phase component is given by:

(12) $q_{1\phi}'' = h_{1\phi}(1 - A_b'')(T_w - T_l)$

with:

T_w = wall temperature

T_l = liquid temperature

A_b'' = fraction of heated surface exposed to boiling

$h_{1\phi}$ = boiling heat transfer coefficient

The boiling heat transfer coefficient is evaluated as:

(13) $h_{1\Phi} = \rho_l c_{p,l} St_l u_l$

while the fraction of the heated surface exposed to boiling is expressed as:

(14) $A_b'' = n'' \varepsilon A_b$

where

A_b = bubble cross-section, defined as $A_b = \pi \frac{{D_b}^2}{4}$

ε = correction coefficient, defined as $\varepsilon = \frac{2\rho_v h_{fg} D_b f}{3 q_w''}$

where f is the nucleation frequency. The boiling component including evaporation and quenching is given by:

(15) $$q_b'' = A_b'' \frac{h_{lg}}{h_{fg}} q_w''$$

It is interesting to notice that, substituting the expression (14) into (15), the boiling component becomes:

(16) $q_b'' = n'' f \frac{\pi D_b^3}{6} \rho_v h_{lg}$

which is equivalent to the formulation of the original Kurul-Podowski model for the evaporative heat flux only. The nucleation site density n" is evaluated with the following correlation:

(17) $n'' = \kappa \left(T_w - T_w^{min}\right)^2$

where κ is a coefficient, and:

$T_w^{min} = T_{sat} + \Delta T_w^{min}$

ΔT_w^{min} = minimum wall superheat at the onset of nucleation, defined according to:

(18) $\Delta T_w^{min} = T_w^{min} - T_{sat} = 2\sqrt{\frac{2\sigma q_w'' v_{fg} T_{sat}}{k_l h_{fg}}}$

3.2 STAR-CCM+ reference boiling models

Before proceeding with the implementation of the new RPI model within the STAR-CCM+ platform, a comparison between the new RPI model as implemented in NPHASE and the reference model currently available in STAR-CCM+ has been performed, and their performance has been evaluated against the Bartolomei experiment.

It has to be pointed out that a variety of models are available within the STAR-CCM+ code and that users are left with the task of selecting the appropriate correlations for the given case under investigation. The following correlations were selected to assemble what here we refer to as the STAR-CCM+ reference model:

- the bubble hydrodynamics was computed by including lift, drag (Wang's correlation), virtual mass, and turbulent dispersion forces;
- the heat partitioning was computed according to the original Kurul-Podowski model, consisting of three separate components;
- the heat transfer coefficient from the gas-liquid interface to the liquid is evaluated according to the Ranz-Marshall correlation expressed as:

(19) $$Nu = 2 + 0.6 Re_d^{0.5} Pr_c^{0.3}$$

- as in the case of the new RPI model, the heat transfer between the gas-liquid interface and the gas phase is assumed to be null;
- the bubble departure diameter is estimated with the Tolubinski Konstanchuk correlation, specifically developed for subcooled liquid:

(20) $$d_w = d_0 \exp\left[-\frac{\Delta T_{sub}}{\Delta T_0}\right]$$

where d_o is a reference diameter (default equal to 0.6 mm), ΔT_o is the reference subcooling (default equal to 45K), and ΔT_{sub} is the subcooling of the liquid next to the wall;

- the bubble departure frequency is given by the Cole's correlation:

(21) $$f = \sqrt{\frac{4}{3}\frac{g(\rho_l - \rho_g)}{d_w \rho_l}}$$

which is equivalent to taking a typical bubble rise velocity (estimated using unit drag coefficient as the velocity scale, over the bubble diameter as the length scale);

- the nucleation site density is given by the Lemmert-Chawla correlation:

(22) $$\frac{n''}{[m^{-2}]} = (m \Delta T_{sup})^p$$

where m is a calibration constant (equal to 185 K^{-1}), p is a superheat exponent (default equal to 1.805), ΔT_{sup} is the wall superheat given by $\Delta T_{sup} = T_w - T_{sat}$.

For the Bartolomei experiment, consistently with the new RPI-NPHASE model, it is further assumed that the bubble diameter is constant and equal to 0.75mm and that the lift coefficient C_L is equal to 0.03.

4 ASSESSMENT OF BOILING MODELS AGAINST EXPERIMENTS

4.1 Comparison of STAR-CCM+ reference model with RPI-NPHASE

Before proceeding with the implementation and validation of the new RPI model in STAR-CCM+, the reference STAR-CCM+ boiling models is assessed against the new RPI model as originally implemented by RPI team in the NPHASE code.

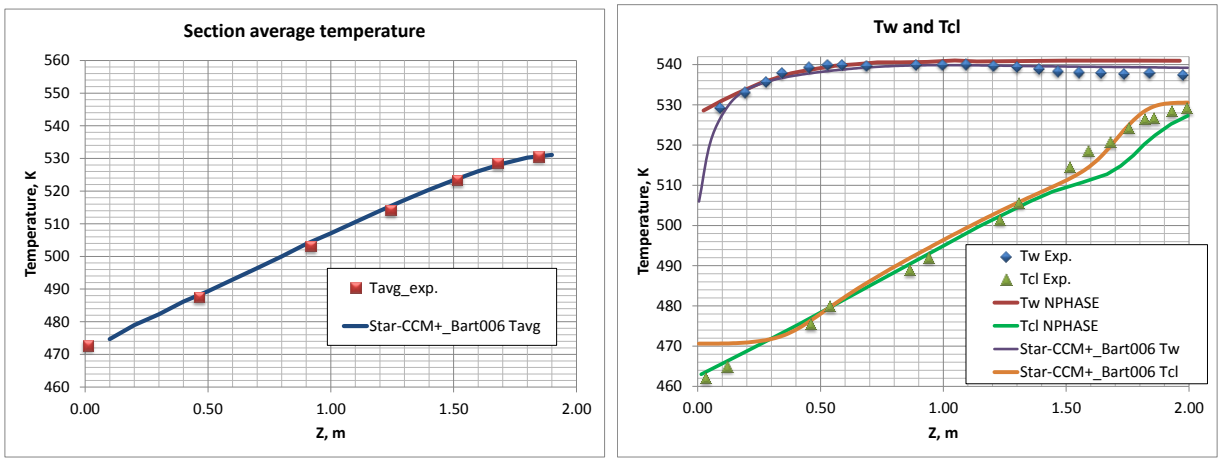

Figure 3: Performance of the new RPI model implemented in NPHASE and the reference STAR-CCM+ model against the Bartolomei experiment. Left: cross-section averaged liquid temperature as function of elevation; right: wall temperature (Tw) and liquid centerline temperature (Tcl) as function of elevation.

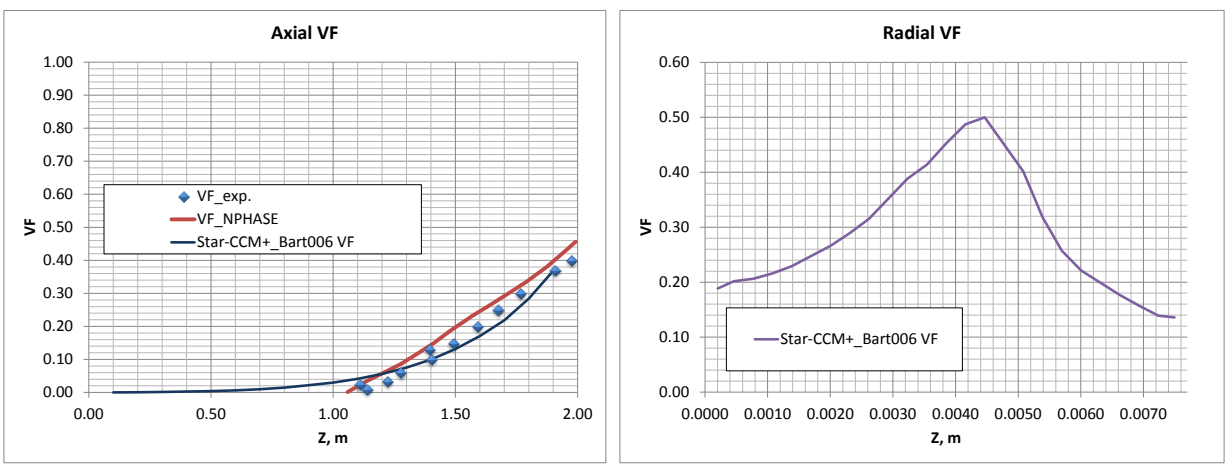

Figure 4: Performance of the new RPI model implemented in NPHASE and the reference STAR-CCM+ model against the Bartolomei experiment. Left: cross-section averaged void fraction as function of elevation; right: void fraction radial distribution at the test section outlet.

The comparison of the new RPI-NPHASE model and the STAR-CCM+ reference model is reported in Figure 3 and Figure 4. The two models are evaluated against data measured by Bartolomei. In Figure 3 the cross-section averaged liquid temperature (left), the wall temperature T_W and the coolant center-line temperature T_{cl} (right) are reported along the test section vertical

axis. In Figure 4 the cross-section averaged void fraction distribution along the test section vertical axis (left) and the void fraction radial distribution at the test section outlet (right) are reported.

Overall, both models seem to perform reasonably well against the Bartolomei experiment. The STAR-CCM+ reference model gives a better prediction of the center-line fluid temperature in the upper part of the test section.

4.2 Implementation of the new RPI model in STAR-CCM+ and assessment against Bartolomei's experiment

In order to systematically investigate the impact of adopting the new RPI correlations on the overall model performance, the implementations of the new RPI model within STAR-CCM+ has been carried out by sequentially substituting the STAR-CCM+ reference model correlations with the ones proposed by RPI.

At first, the Ranz-Marshall correlation for the heat transfer from the gas-liquid interface to the liquid is replaced with eq. (10). A coefficient $C_{vol} = 2$ has been assumed. As can be seen in Figure 5 and Figure 6, the replacement of the heat transfer correlation has some minor effect on the cross-section averaged void fraction distribution and on the liquid center-line temperature, but the wall temperature seems to remain unaffected by the change.

The replacement of the bubble departure diameter correlation (see Figure 7 and Figure 8) is strongly affecting the radial void fraction distribution (for a given set of bubble forces correlations). The wall temperature was unaffected by the change, for this particular case.

The results obtained by replacing the heat partitioning model, i.e. with the full implementation of the new RPI model in STAR-CCM+ are presented in Figure 9 and Figure 10. Overall the new model and the reference model perform equally well for the Bartolomei experiment. The wall temperature seems to be affected mainly by the bubble nucleation site density model. The only significant difference is found in the void fraction radial distribution for which no experimental data is available.

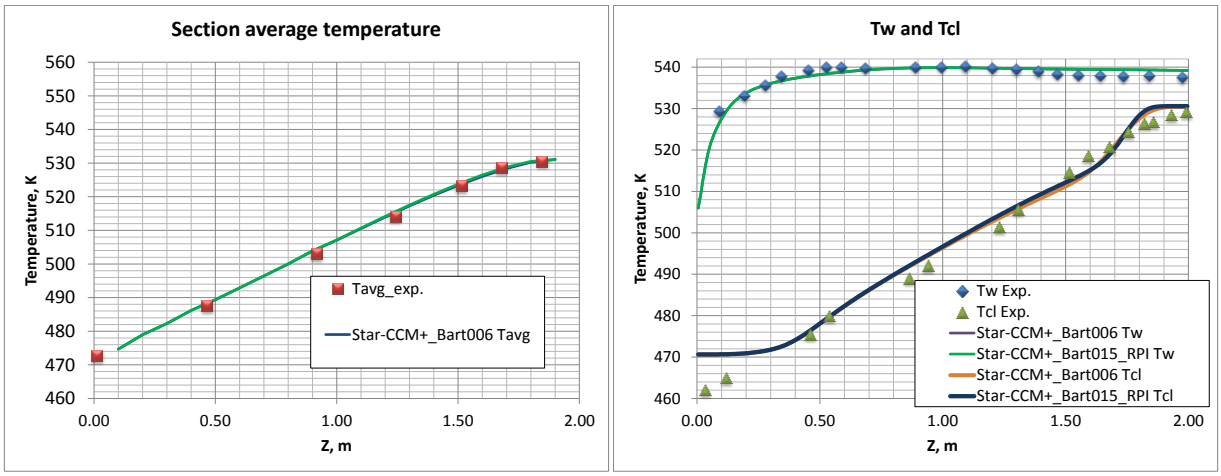

Figure 5: Performance of the new RPI model implemented in STAR-CCM+ and STAR-CCM+ model against the Bartolomei experiment - effect of gas-liquid interface to liquid heat transfer on liquid and wall temperatures.

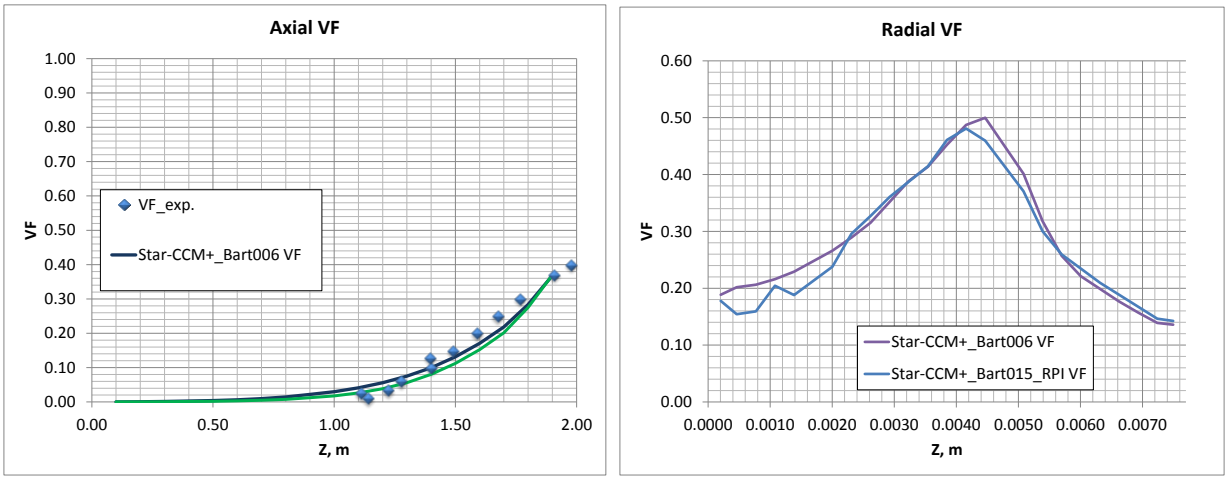

Figure 6: Performance of the new RPI model implemented in STAR-CCM+ and STAR-CCM+ model against the Bartolomei experiment - effect of gas-liquid interface to liquid heat transfer on the void fraction.

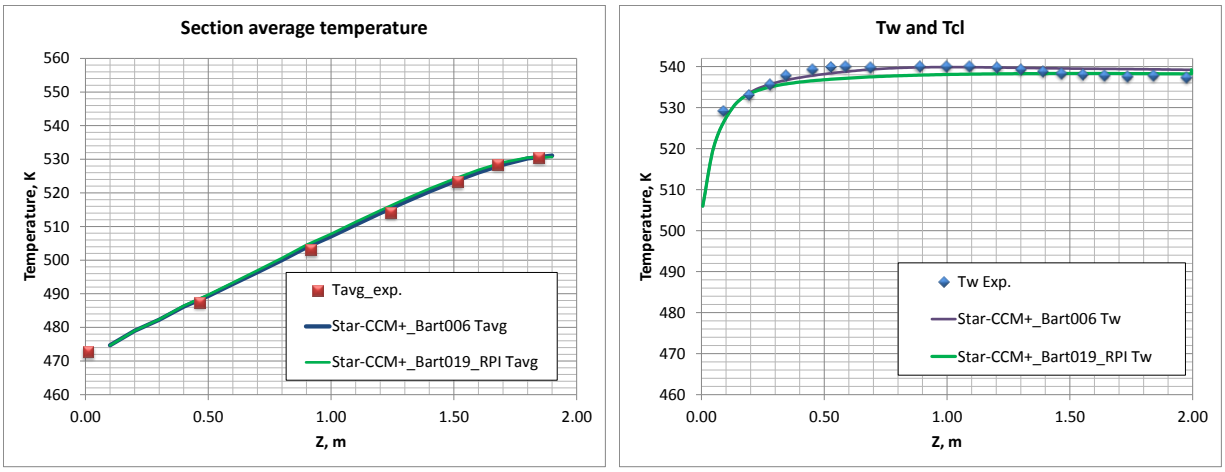

Figure 7: Performance of the new RPI model implemented in STAR-CCM+ and STAR-CCM+ model against the Bartolomei experiment - effect of bubble departure diameter on liquid and wall temperatures.

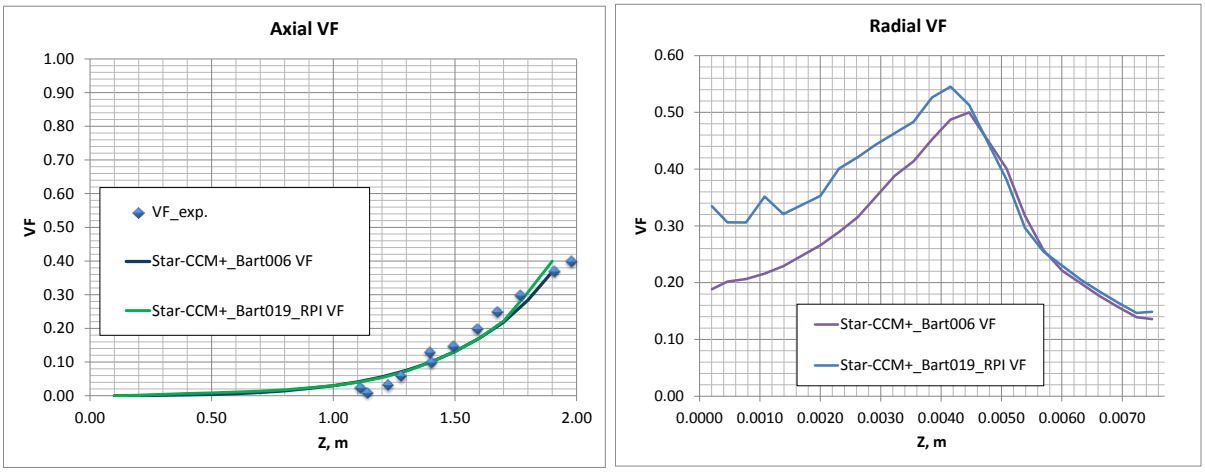

Figure 8: Performance of the new RPI model implemented in STAR-CCM+ and STAR-CCM+ model against the Bartolomei experiment - effect of bubble departure diameter on the void fraction.

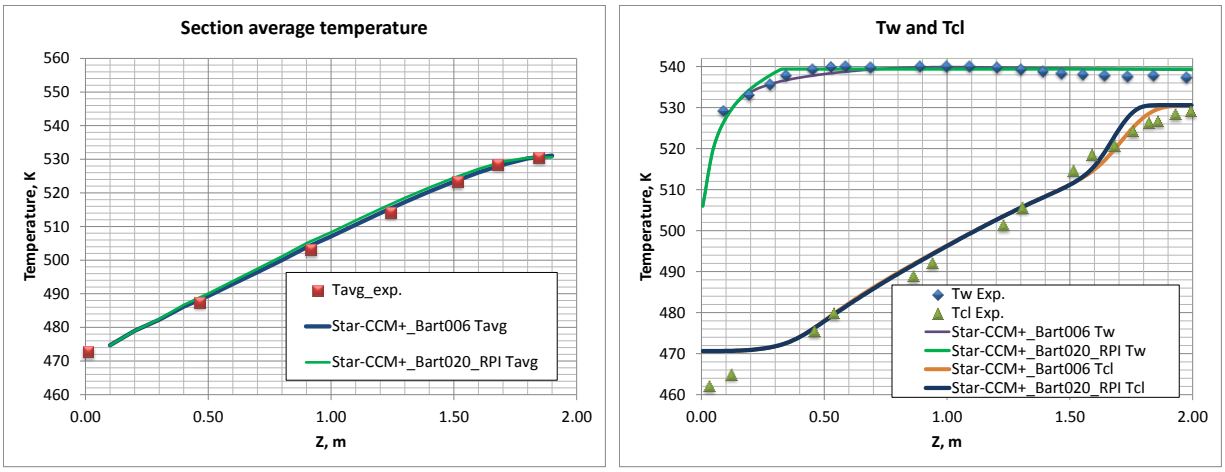

Figure 9: Performance of the new RPI model implemented in STAR-CCM+ and STAR-CCM+ model against the Bartolomei experiment - effect of heat partitioning on liquid and wall temperatures.

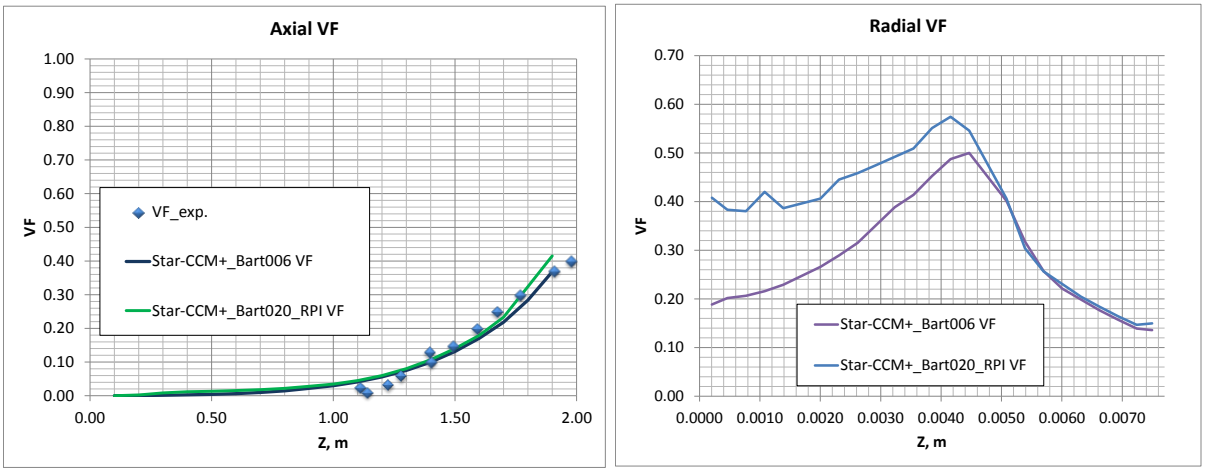

Figure 10: Performance of the new RPI model implemented in STAR-CCM+ and STAR-CCM+ model against the Bartolomei experiment - effect of heat partitioning on the void fraction.

4.3 Implementation of the new RPI model in STAR-CCM+ and assessment against selected DEBORA's experiments

As for the assessment against the Bartolomei's experiment, a sequential implementation of the new RPI's correlations has been carried out and the results compared against selected DEBORA's experimental data. Seven steps have been executed:

- #01 – CCM+ reference boiling model, with constant bubble diameter equal to 0.5 mm (according to experimental data), Ranz-Marshal correlation for the heat transfer from the gas-liquid interface to the liquid, Cole's correlation for the bubble departure frequency, Del Valle's correlation for the bubble-induced quenching, Wang curve for the drag force, Lemmert-Chawla's correlation for the nucleation site density, Tulubinsky's correlation for the bubble departure diameter; bubbles are assumed to be spherical. Forces: virtual mass

force (no lift, no wall lubrication); this is equivalent to the reference case already discussed in chapter 4.2.

- #02 –same as #01 but employing Bozzanno-Dente 's correlation for the drag force, without drag correction;
- #03 – RPI correlation for Nusselt numbers for gas and liquid phases, Wang curve for drag force; bubbles are assumed to be spherical; this is equivalent to case v015 discussed in chapter 4.2.
- #04 –same as #03 but using Bozzanno-Dente 's correlation for the drag force, without drag correction;
- #05 – same as #3 with RPI's new model for the bubble departure diameter and heat partitioning model; this is equivalent to case v019 discussed in chapter 4.2.
- #06 - same as #05 but with Bozzanno-Dente 's correlation for the drag force, without drag correction;
- #07 – complete RPI model, including RPI bubble departure frequency; this is equivalent to case v020 discussed in chapter 4.2.
- #08 – complete RPI model with Bozzanno-Dente 's correlation for the drag force, without drag correction.

The Bozzano-Dente's correlation [7] gives the following expression for the drag coefficient:

$$C_D = f\left(\frac{a}{R_0}\right)^2 \tag{23}$$

where f is a friction factor and (a/Ro) is a deformation factor given respectively by:

$$f = \left(\frac{48}{\mathrm{Re}}\right)\frac{1 + 12\mathrm{Mo}^{1/3}}{1 + 36\mathrm{Mo}^{1/3}} + 0.9\frac{\mathrm{Eo}^{3/2}}{1.4(1 + 30\mathrm{Mo}^{1/6}) + \mathrm{Eo}^{3/2}} \tag{24}$$

.

$$\left(\frac{a}{R_0}\right)^2 \cong \frac{10(1 + 1.3\mathrm{Mo}^{1/6}) + 3.1\mathrm{Eo}}{10(1 + 1.3\mathrm{Mo}^{1/6}) + \mathrm{Eo}} \tag{25}$$

In eq. (25) Mo is the bubble Morton number, and Eo is the Eotvos number. Bozzano-Dante's correlation is recommended for bubble flow regimes in a wide pressure range.

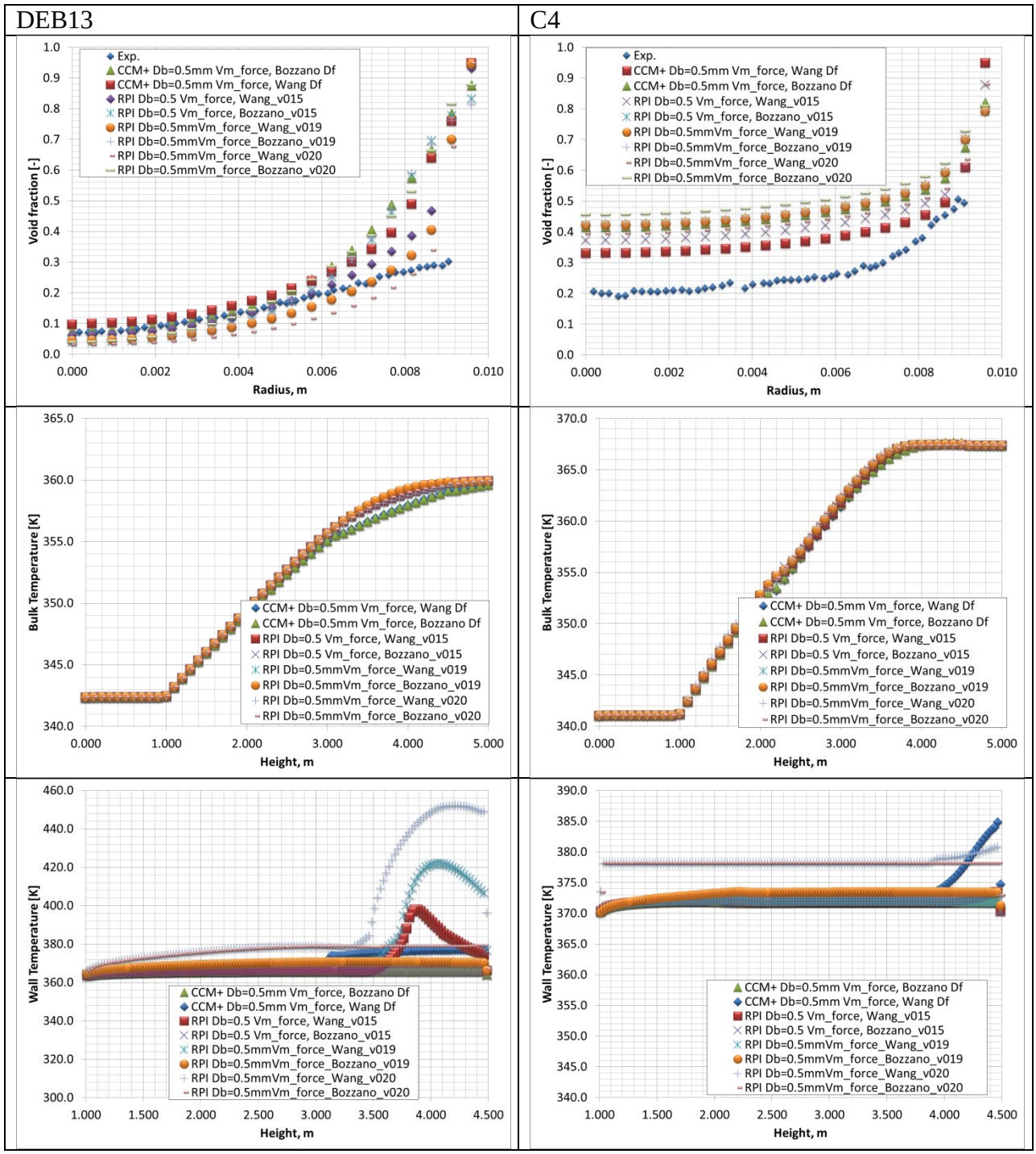

Figure 11: Computational results for DEB13 (left) and C4 (right) cases.

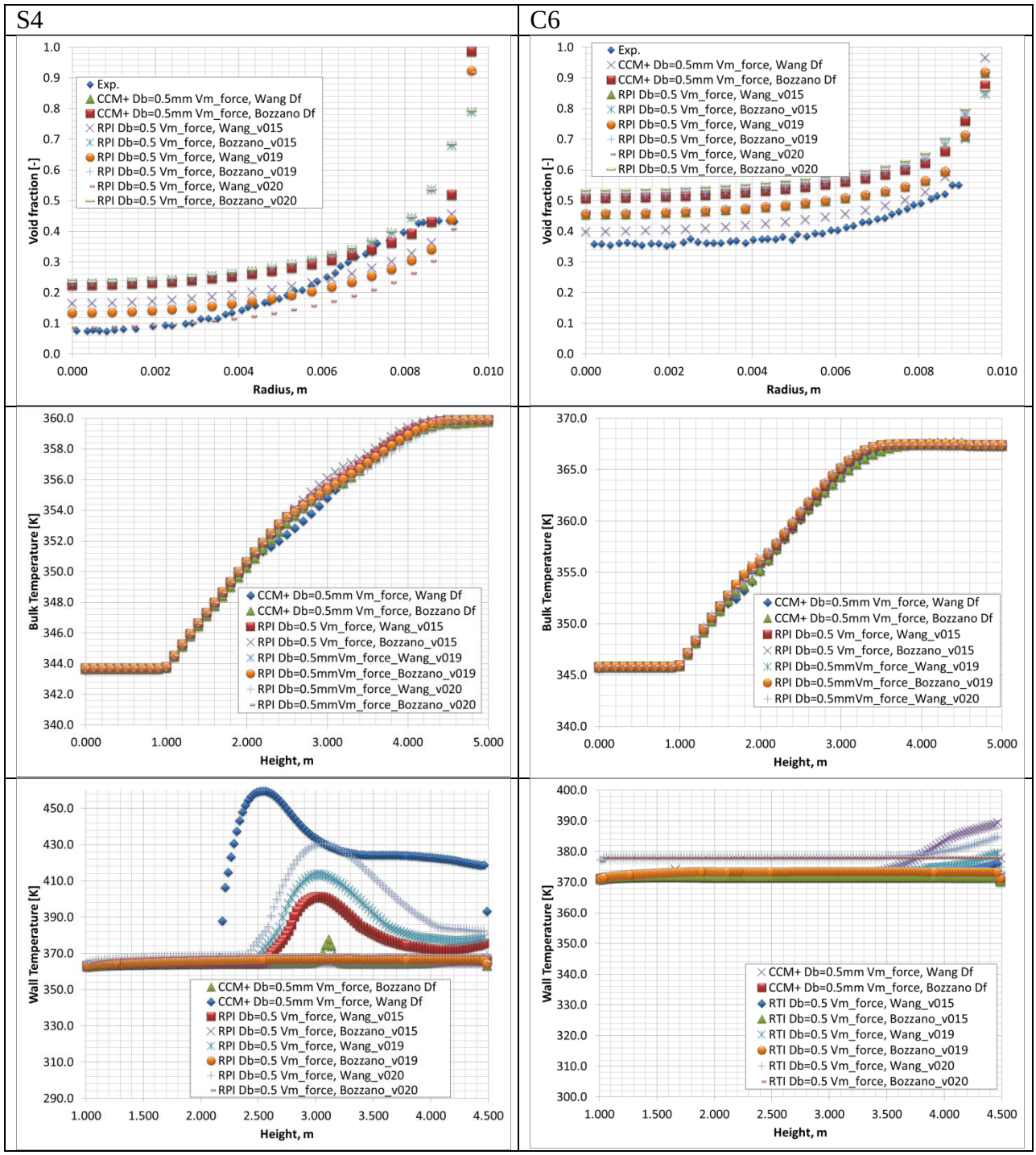

Figure 12: Computational results for S4 (left) and C6 (right) cases.

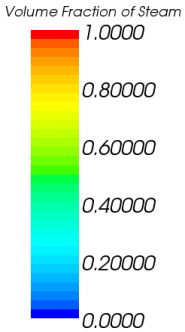

Figure 13: Color bar for Figure 14 to Figure 16.

The results obtained with the different modeling options #01-#08 for the selected DEBORA cases listed in Table 1 are reported in Figure 11 and Figure 12. The contour plots of the void-fraction on the pipe vertical cross-section are reported in Figure 14 to Figure 17, with corresponding color bar shown in Figure 13.

By observing the void-fraction radial profiles (top pictures in Figure 11 and Figure 12), it can be concluded that the heat partitioning model and the Nusselt correlation for the heat transfer between the two-phase interface and the liquid phase have practically no influence on the overall shape of the void-fraction profile.

As expected, the shape of the radial void-fraction profile is mainly dictated by the force balance in the radial direction. The heat transfer models have however influence on the absolute values of the local void fractions. By analyzing the results obtained for the four DEBORA cases of Table 1, no clear conclusion can be drawn on the improvements introduced by the RPI model. The new RPI model appears to perform better than current models for case DEB13 and S4, but does not perform as well for cases C4 and C6.

The bulk coolant temperature is not sensitive to the particular heat partitioning and Nusselt correlations. The only deviation appears when the Wang correlation for the drag force causes an unphysical rise of the wall temperature. It has to be notice however that the Wang correlation was originally developed for air-water flows close to atmospheric pressure.

For the DEBORA cases analyzed here, it is noticed that the wall temperature is very sensitive to the bubble departure frequency (see the change in Figure 11 and Figure 12 from case v19 to v20). Unfortunately, no wall temperature measurements are available for these tests. It is worthwhile noticing that this high sensitivity of the wall temperature to the bubble departure frequency correlation was not observed with the Bartolomei's case discussed in chapters 4.1 and 4.2.

In addition, unphysical local wall superheat (see Figure 18) was observed in some of the cases. This issue has been reported to the two-phase model developers team of CD-Adapco, but to date no clear cause has been found.

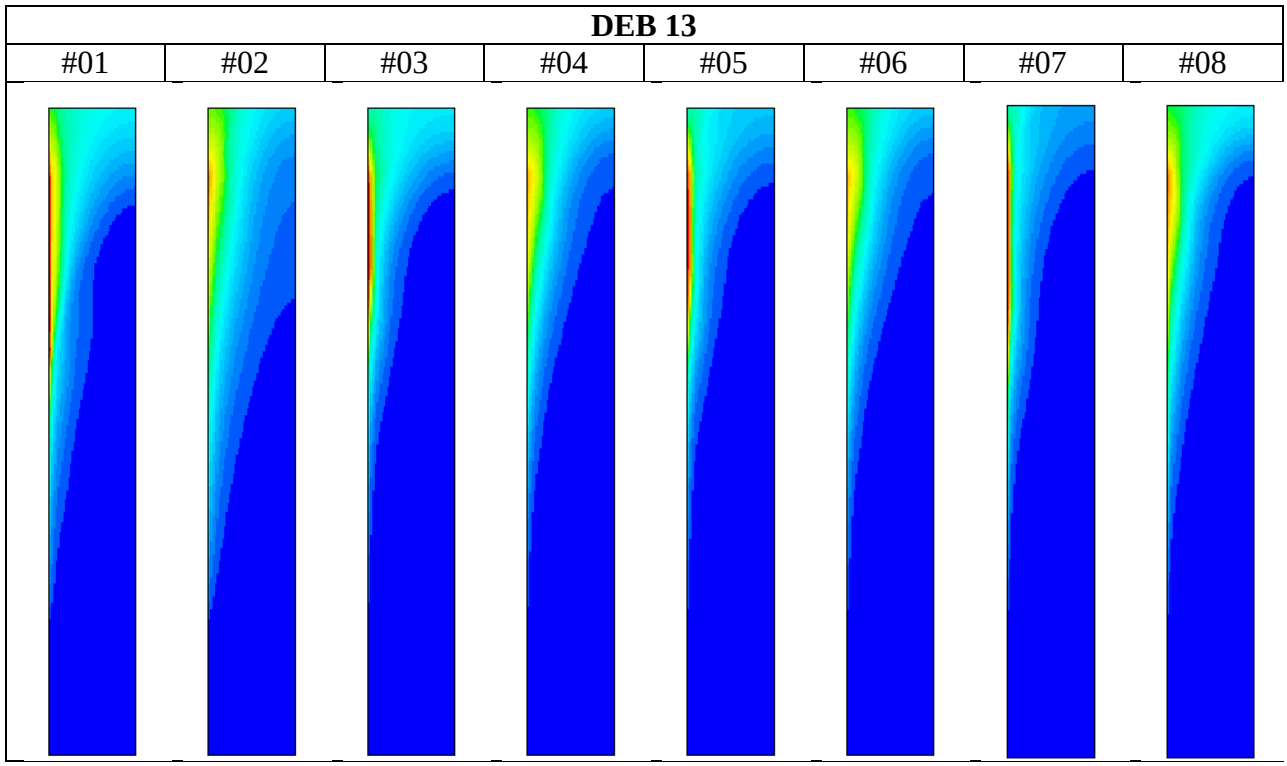

Figure 14: Void-fraction profiles for different variants of boiling models – DEB13

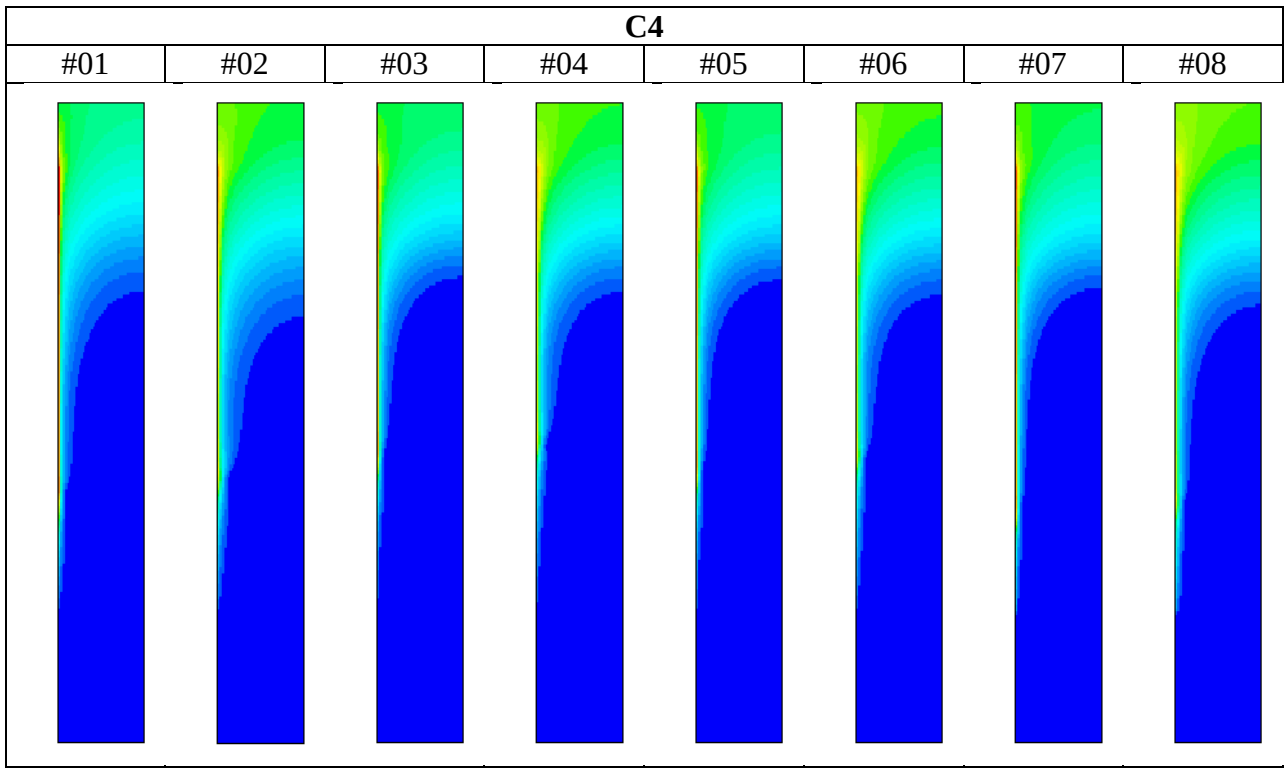

Figure 15: Void-fraction profiles for different variants of boiling models - C4

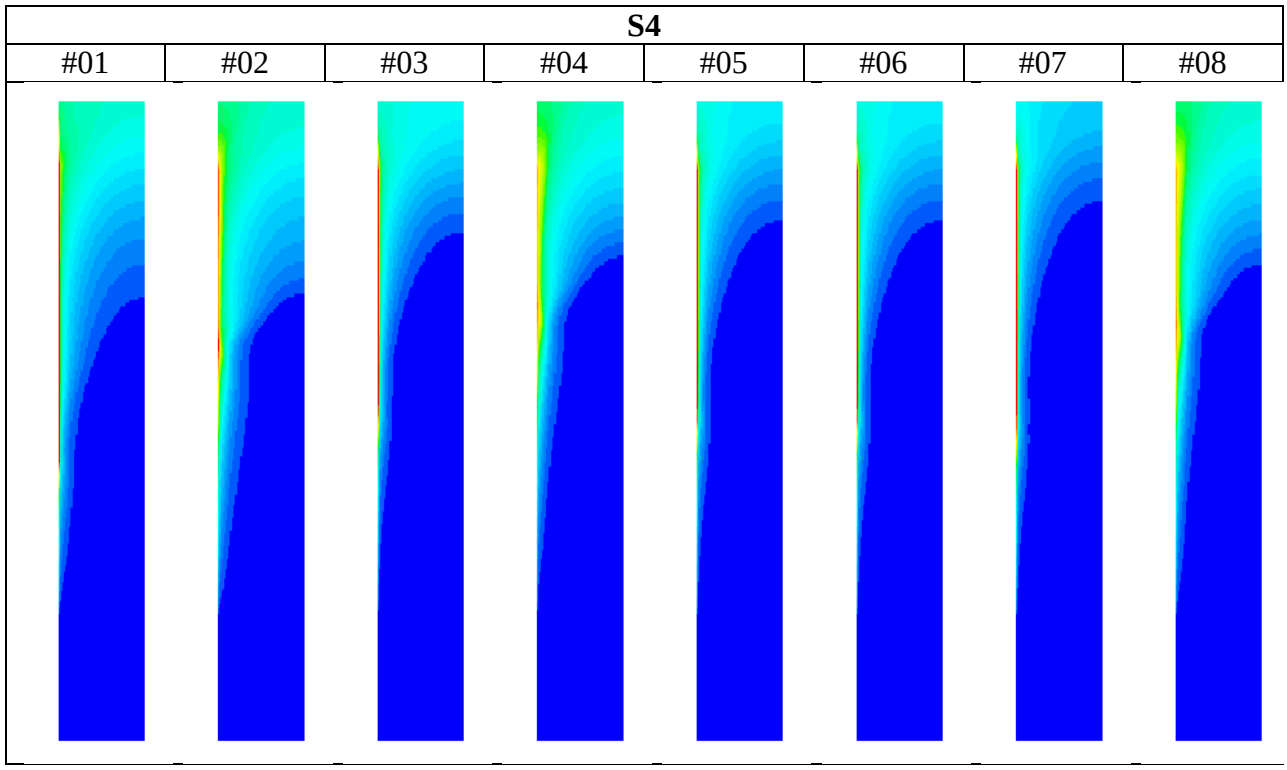

Figure 16: Void-fraction profiles for different variants of boiling models - S4

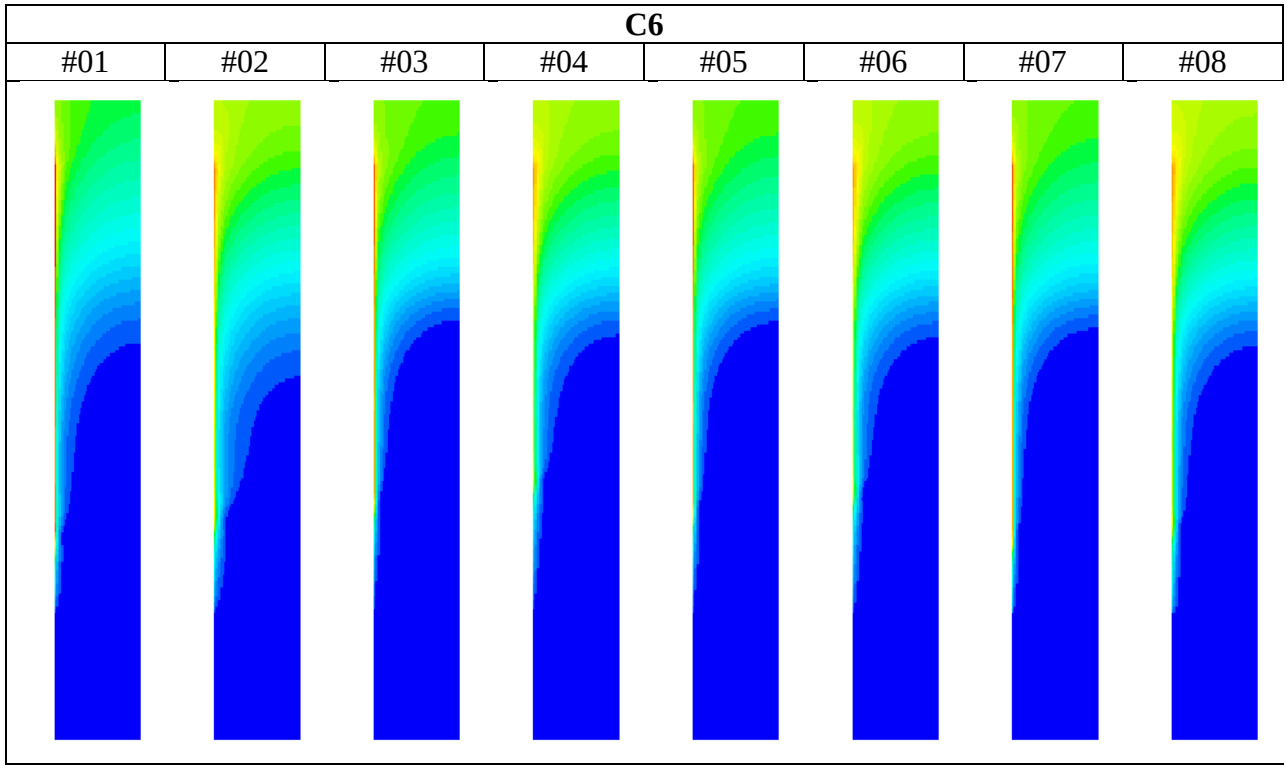

Figure 17: Void-fraction profiles for different variants of boiling models – C6

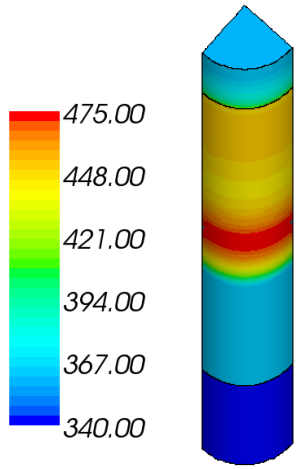

Figure 18: Wall temperature profile for case S4 model variant #02 (STAR-CCM+ reference model with Bozzano-Dante's correlation for the drag coefficient).

5 CONCLUSIONS AND FUTURE WORK

It can be concluded that:

- the model shows a reasonable level of maturity and is ready for implementation in the VERA T/H tools, namely Hydra-TH;
- the evaluation of the model has confirmed the expected sensitivity on model parameters and further improvements are to be expected during the V&V phase;
- the comparison with the STAR-CCM+ reference closure against the Bartolomei experiment presented here and the previous work on PSBT and DEBORA experiments confirm that we have a robust base for the VERA tools;
- the work has clearly been limited to PWR targeted application and there is still work to do to extend it outside of this area;
- last but not of least importance, the comparison of model results against Bartolomei, DEBORA and PSBT experiments have highlighted a serious drawback of the experiments currently available in the open literature. While some experiments (e.g. Bartolomei) provide good data for the wall temperature but lack detailed void-fraction distributions, other experiments (e.g. DEBORA, PSBT) provide detailed void fraction distributions, but no wall temperatures. A sound model validation would require knowledge of both quantities.

6 REFERENCES

1. Bartolomei, G.G. and Chanturia, V.M., 1967, "Experimental Study of True Void Fraction when Boiling Subcooled Water in Vertical Tubes", Thermal Engineering, Vol. 14, pp.123-128.Garnier, J., Manon, E., Cubizolles, G., 2001. Local measurements on flow boiling of refrigerant 12 in a vertical tube. Multiphase Science and Technology, 13, 1–111.

2. Garnier, J., Manon, E., Cubizolles, G., 2001. Local measurements on flow boiling of refrigerant 12 in a vertical tube. Multiphase Science and Technology 13, 1–111.
3. Shaver, D.R., Antal, S.P., Podowski, M.Z., 2013. Modeling and analysis of interfacial heat transfer phenomena in subcooled boiling along PWR coolant channels. Proceedings of the NURETH-15 conference, Pisa, Italy, May 12 - 16.
4. Shaver, D.R., Antal, S.P., Podowski, M.Z., 2012. Multidimensional mechanistic modeling of interfacial heat and mass transfer. Proceedings of the ICAPP'12 conference, Chicago, IL, June 24 - 28.
5. Jiao, H., Podowski, M.Z., 2012. An analysis of multidimensional models of gas/liquid flows. Proceedings of the ANS Winter Mtg, San Diego, CA, Nov 11 - 15 (PPT slides).
6. Podowski, M.Z., 2012. Toward mechanistic modeling of boiling heat transfer. Nuclear Engineering and Technology, Vol. 44, no. 8.
7. Bozzano, G., and Dente, M. 2001. Shape and terminal velocity of single bubble motion: a novel approach. Computers and Chemical Engineering, 25, pp. 571-576.